Optimizing Equivalent Circuit Model Parameters of DFB Lasers With RSM Model and NSGA-II Algorithm

Qing-an Ding, Xudong Cheng, Huixin Liu, Xiaojuan Wang, Xiaohan Guo, Li Zheng, Junkai Li, Zhenfei Dai, Qunying Yang, and Jun Li

***Abstract*—The parameters group of the distributed feedback (DFB) laser equivalent circuit model based on the single-mode rate equations is the key to precisely presenting DFB response characteristics, so a novel optimization solution based on the response surface methodology (RSM) is proposed to rapidly select the optimized parameters by the multi-objective algorithm. The RSM model is designed to match the DFB laser characteristics related to the direct-current and small-signal frequency response, and non-dominated sorting genetic algorithm-II (NSGA-II) attributes to elevating the RSM model optimizing to screen out an optimal set of parameters by Pareto sorting. To further verify the accuracy of the model, the resonant frequency (f_r) and the threshold current (I_{th}) are considered the objective optimization variables to set the target values as 18 GHz and 11.5 mA. The single-objective and multi-objective optimization are analyzed and compared to each other, and the optimized results have shown good agreement with predicted values, such as lower I_{th} in the multi-objective optimization while close f_r in both cases. It has been demonstrated that optimization makes it possible not only to exploit the potential of existing DFB lasers but also to provide guidance for the inverse design of laser.**

***Index Terms*—DFB laser, parameter optimization, response surface methodology (RSM), non-dominated sorting genetic algorithm-II(NSGA-II), Pareto sorting, multi-objective optimization.**

Manuscript received 14 July 2022; revised 7 August 2022; accepted 19 August 2022. Date of publication 23 August 2022; date of current version 9 September 2022. This work was supported in part by Shandong Natural Science Foundation, China under Grants ZR2017MF070, ZR2020MF014, and ZR202103060092, in part by the National Natural Science Foundation of China under Grants 61471224 and 61801267, and in part by the Scientific Research Foundation of Shandong University of Science and Technology for Recruited Talents under Grant skr-D-0104060540915. *(Corresponding author: Xiaohan Guo.)*

Qing-an Ding is with the School of Electronics and Information Engineering, and also with the Director of Microwave and Optical Communication Studio, Shandong University of Science and Technology, Qingdao 266510, China (e-mail: aqd6677@126.com).

Xudong Cheng, Huixin Liu, Xiaojuan Wang, Li Zheng, Junkai Li, Zhenfei Dai, Qunying Yang, and Jun Li are with the Microwave and Optical Communication Studio, and also with the College of Electronic Information Engineering, Shandong University of Science and Technology, Qingdao 266510, China (e-mail: 480346326@qq.com; 2895187400@qq.com; 1023710441@qq.com; 3449950944@qq.com; 2261236194@qq.com; 1598559691@qq.com; 642864604@qq.com; lijun08022021@163.com).

Xiaohan Guo is with the School of Information Science and Engineering, Shandong University Qingdao, Qingdao 266237, China (e-mail: first18953266801@126.com).

Digital Object Identifier 10.1109/JPHOT.2022.3201109

I. Introduction

As A key component of the optical fiber communication system, a high-speed modulation semiconductor laser with excellent modulation performance is the premise for improving the speed of optical fiber communication [1], [2], [3], [4]. Laser modeling and adjusting design parameters through simulation are the key steps before laser production. Theoretically, without taking into account the optical phase, the theory of rate equations is sufficient to describe the response characteristics of semiconductor lasers [5], [6]. Using an equivalent circuit model, characterizing distributed feedback (DFB) lasers based on rate equations is a constant preoccupation. Meanwhile, precise model parameters have become a concentrated issue in obtaining reliable simulation results during DFB laser simulation [7].

In recent years, there has been a growing interest in laser parameter optimization [8], [9], [10], [11], [12]. The most research subject has been strictly limited the direct laser's structural parameters optimization, including optimizing the doping and dimensional parameters of the active region to increase the modulation bandwidth [13], [14], [15], [16], [17]. Nowadays, GA are widely used in optics field, especially to improve the output performance of lasers [18], [19]. Wei Quan used GA to obtain the relationship between power, wavelength, current and temperature in order to obtain wavelength and power predictions from the distributed Bragg reflection lasers [20]. E. J. R. Kelleher used GA to intelligently locate optimal parameters for stable single-pulse mode-locking in a figure-of-8 fiber laser and to monitor both temporal and spectral output properties of the laser [21].

The specific purpose of laser parameter optimization is to achieve the best response characteristics by searching for the optimal parameters. Many researchers regard optimization as a multi-parameter non-linear problem and attempt to find a non-linear function to depict the relationship between the parameters and the responses [22], [23], [24], [25]. The development of numerical methodology has made it possible to perform complex nonlinear optimization with acceptable accuracy in a relatively short period of time. Therefore, the parameter optimization of the laser equivalent circuit model can be transformed into a mathematical modeling process, so the optimal parameters can be obtained by applying the function optimization method [26],

[27]. However, model convergence is not optimal due to the stochastic nature of the numerical optimization method. Hence, it could be critical to constrain the optimized parameters.

In this paper, in order to realize the inverse design of DFB laser, a new parameter optimization method is developed to directly optimize the equivalent circuit model parameters by combining response surface methodology (RSM) and non-dominated sorting genetic algorithm-II (NSGA-II). Initially, the parameters to be optimized are determined based on the laser response characteristics in terms of the rate equations. Afterwards, a multiple regression equation is applied to fit the relationship of the parameters to the response. Besides, a RSM model is introduced to accurately approach the DFB laser response characteristics with a simple and effective process. The accuracy of the model is verified by the variance analysis of the RSM model. We employ non-dominated sorting genetic algorithm-II (NSGA-II) to optimize the model and search for feasible solutions by Pareto ranking, and the optimized parameters substituted into the equivalent circuit model have consistent response characteristics with the RSM predicted result. In addition, a single-objective optimization focused solely on resonant frequency (f_r) and a multi-objective optimization taking into account both f_r and the threshold current (I_{th}) are compared and analyzed. The simulation results show that the multi-objective optimization significantly improves the comprehensive performance of the DFB laser due to the consideration of the influence on the threshold current by the optimized parameters. The method demonstrates that under ideal conditions, the RSM model can replace the laser equivalent circuit model for inverse design of parameters with high predictability. In addition, it can provide design guidance for different types of lasers due to its generality.

II. Theory

A. Single-Mode Rate Equations of DFB Laser

The rate equation is a dynamic equation that characterizes the density variations of the carrier and the photon in the active region of a laser. By building an equivalent circuit model based on the rate equations, the static and dynamic characteristics of the laser's active region can be described [28], [29].

$$\frac{dN}{dt} = \frac{I_{\mathrm{j}}}{qV} - R_{\mathrm{n}}(N) - R_{\mathrm{r}}(N) - \frac{g_0\,(N-N_0)}{1+\varepsilon S}S, \quad (1)$$

$$\frac{dS}{dt} = \Gamma\frac{g_0\,(N-N_0)}{1+\varepsilon S}S + \Gamma\beta R_{\mathrm{r}}(N) - \frac{S}{\tau_{\mathrm{p}}}. \quad (2)$$

Here, N is active-region carrier density, I_j is the time-dependent injected current, q is the electron charge, V is the active region volume, $R_{\mathrm{n}}(N)$ is the rate of nonradiative recombination, $R_{\mathrm{r}}(N)$ is the rate of radiative recombination, g_0 is the differential gain coefficient, N_0 is the carrier density at transparency, ε is the optical-gain-compression factor, S is the photon density, Γ is the optical-confinement factor, β is the spontaneous-emission factor, and τ_p is the photon lifetime.

Eq. (1) and (2) are two standard circuit equations by which the intrinsic circuit model of the laser can be completely constructed. However, the operation of the laser requires not only the intrinsic laser chip but also the support of external circuits. Since the package parasitic effect occurs when the chip and the external circuit are coupled and matched, as shown in Fig. 1, our team has developed an improved circuit model considering the following package parasitic parameters: (1) space-charge capacitance C_{sc}; (2) bleeder resistance R_d; (3) parasitic shunt capacitance C_p and series resistance R_s introduced by the chip and electrode contact; (4) parallel capacitance C_a introduced when the chip electrode contacts the carrier; (5) inductive L_a and resistive R_a presented by the gold wire connecting the chip to the external circuit. In this way, the simulation results of the model will be more realistic and reliable. It is worth stating that in this study, the effects of optical phase on the carrier density and output power of the laser are neglected.

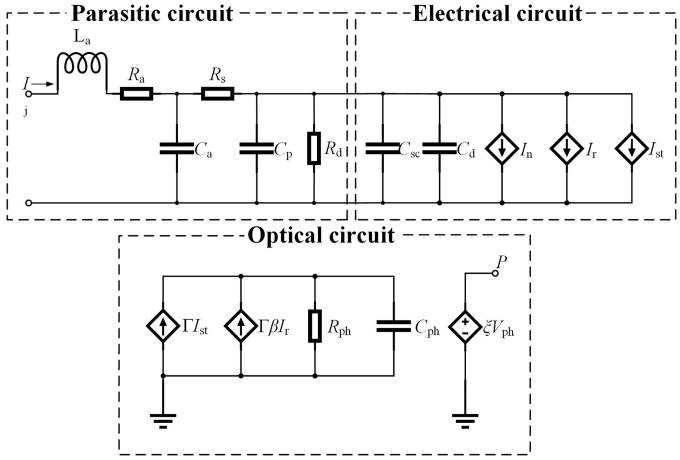

Fig. 1. Schematic diagram of the equivalent-circuit model for a high-speed DFB laser. It includes three parts: parasitical circuit, electrical circuit, and optical circuit.

In electrical circuit, C_d is the diffusion capacitance at junction, I_{st}, I_r and I_n represent currents in different recombination processes. In optical circuit, V_{ph} has a voltage dimension, which indicates the light pressure in the active region. C_{ph} has capacitance dimension, which can be equivalent to a capacitor, and R_{ph} has resistance dimension, which can be equivalent to a resistor. Their specific expressions are given by $C_d = (qVN_e/\eta V_T)\exp(V_j/\eta V_T)$, $I_n = qVR_n(N)$, $I_r = qVR_r(N)$, $I_{st} = qVS(g_0(N-N_0)/(1+\varepsilon S))$, $V_{ph} = SVV_T$, $C_{ph} = q/V_T$ and $R_{ph} = V_T\tau_p/q$. Where $V_T = KT/q$. Using the equivalent circuit model built in the circuit simulation software PSpice, the direct-current optical output power (P-I) characteristics and frequency response characteristics of the laser can be analyzed.

Generally, the P-I curve allows to determine the threshold current and external differential quantum efficiency of the laser, etc. When the applied forward current reaches a certain value, the output optical power increases sharply and laser oscillations will occur. The threshold current can be written as:

$$I_{th} = \frac{qVN_{th}}{\tau_n}, \quad (3)$$

where τ_n is the carrier lifetime and N_{th} is the threshold carrier concentration.

$$N_{th} = N_0 + \frac{1}{\Gamma\tau_p g_0}. \quad (4)$$

Simultaneous (5), the threshold current can be rewritten as:

$$I_{th} = \frac{qV}{\tau_n}\left(N_0 + \frac{1}{\Gamma\tau_p g_0}\right). \tag{5}$$

While the bias current is greater than the threshold value and the modulation signal is small enough, the resonant frequency (f_r) of the laser can be approximated as [30]

$$f_r \approx \left(\frac{g_0 S_0}{\tau_p\left(1+\varepsilon S_0\right)}\right)^{1/2}, \tag{6}$$

where S_0 is the steady-state photon density.

To quantify the threshold current, a refinement of the photon lifetime is performed as shown below.

$$\tau_p = \frac{1}{\nu_g\left[\alpha_{\text{int}} - \frac{\ln(R_L R_R)}{2L}\right]}, \tag{7}$$

where L is the length of the active region, ν_{g} is the group velocity, α_{int} is the intracavity photon absorption coefficient including absorption in the cladding layers and scattering loss, and R_L, R_R are respectively reflectance of left and right end faces.

B. Response Surface Methodology (RSM)

Response surface methodology (RSM) is an analytical function for modeling and predicting an objective response affected by multiple input variables [31]. Assume a study analyzing a process or system contains a response that depends on multiple factors $x_1, x_2, \ldots, x_{\text{n}}$.

$$y = f\left(x_1, x_2, x_3, \ldots, x_n\right) + \varphi \tag{8}$$

The relationship between the response variables and the independent variables (impact factors) in response surface problems as a function of being often ambiguous. We assume that φ is independent of each other in different tests and follows a normal distribution with a mean of 0 and a variance of σ^2.

RSM model is used to approximate the true functional relationship between the response and the impact factors, and then the model is analyzed to search for the best combination of independent variables that brings the response output variable closest to its target value. To make the model more precise, higher-order equations are considered to the extent practicable. The fourth-order expansion of (9) is applied as an approximation to the actual function in a relatively small region [32].

$$y = \alpha_0 + \sum_{i=1}^{n}\alpha_i x_i + \sum_{i=1}^{n}\alpha_{2i}x_i^2 + \sum_{i=1}^{n}\alpha_{3i}x_i^3 + \sum_{i=1}^{n}\alpha_{4i}x_i^4 + \sum_{i\neq j}\beta_{ij}x_i x_j + \varphi \tag{9}$$

where α_i is the linear effect of x_i, $\alpha_{2\,i}$ is the quadratic effect of x_i, $\alpha_{3\,i}$ is the cubic effect of x_i, $\alpha_{4\,i}$ is the quartic effect of x_i, and β_{ij} is the linear interaction between different parameters x_i and x_j.

To check the accuracy and reliability of the RSM, the most important step in fitting the model is to conduct an analysis of variance (ANOVA) according to the constraint range of variables. During the analysis process, correlation coefficient $R^2 = 1 - \sum_{i=1}^{N}\left(f_i - f_i'\right)^2 / \sum_{i=1}^{N}\left(f_i - \bar{f}\right)^2$ and root mean square error $\sigma_{RMSE} = \sqrt{\sum_{i=1}^{N}\left(f_i - f_i'\right)^2 / N - 1}$ are selected as the standards to measure model accuracy, where N is the number of selected simulation data by PSpice, f_i and f_i' are the sample value and approximate model approximation respectively, and $\bar{f}$ is the average value of all samples [27].

In general, the R^2 indicates the percentage of the regression square sum in the total variance, with an optimal value of 1. The σ_{RMSE} indicates the error between the value calculated by the sample point regression method and the directly calculated value, with an optimal value of 0.

In this study, due to the variety of parameters affecting the output characteristics of the DFB laser, five parameters (Γ, g_0, ε, R_L and R_R) to be optimized are selected as the input variables of the RSM model, and the output characteristics (f_r and I_{th}) are set as the optimization target. In order to realize the multi-objective cooperative optimization of the laser, an overview of the theory related to multi-objective optimization is given first.

C. Non-Dominated Sorting Genetic Algorithm-II (NSGA-II)

To accelerate the optimal convergence of the multiple laser parameters, GA is applied to implement multi-objective optimization [33], [34], [35]. The principle of GA is to simulate the process of population evolution of biological populations [36], [37], [38]. Firstly, the objective function is mapped to the fitness function of individuals in the population, which indicates the ability of individuals to adapt to their environment. Then, the offspring populations are generated through genetic operations such as natural selection, crossover, and mutation. Individuals with high fitness are more likely to produce offspring and preserve them, and their offspring populations have better adaptive capacity on average than their parent populations. Finally, through several generations of evolution, the average fitness of the population will converge to the maximum value, and the algorithm will eventually converge to the global optimal point of the objective function. On the basis of the GA genetic algorithm, NSGA-II makes the solution finally distributed uniformly in the Pareto optimal front end by introducing an elite strategy. It ensures that the optimal individuals are always preserved in the process of population evolution and improves the convergence speed of the algorithm. In multi-objective optimization solution process, the optimization objectives may vary for different sub-objective functions, including solving for the maximum value, minimum value, or objective value.

The solutions of multi-objective optimization problems in DFB lasers are normally not unique and have no absolute advantages or disadvantages. Because of the conflicting relationships between resonant frequency and threshold current, it is difficult to optimize both objectives simultaneously. It follows that the main task of laser optimization is to search the parameter solution to make the resonant frequency and threshold current reach the expected value of design, which is called the non-dominated solution set or Pareto optimal solution set. In this current study, the optimization starts with an initial parent population of N candidate solutions. Each candidate solution is a point in a

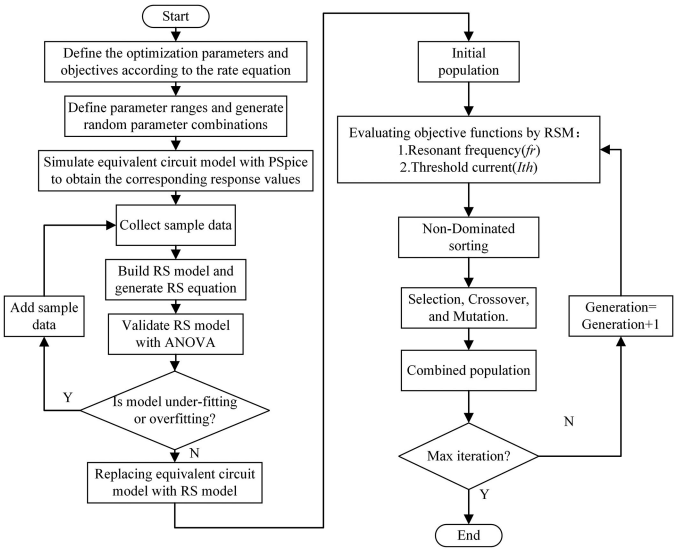

Fig. 2. Flow chart of the proposed optimization approach.

multidimensional space representing a multidimensional vector with a set of DFB parameters to be optimized, also known as genes. Binary coding is applied to the parental populations, and a set of parameters $\Gamma(0.25)$, $g_0(1.42 \times 10^{-12}$ m^3/s), $\varepsilon(13.20 \times 10^{-24}$ m^3), $R_l(0.30)$, and $R_r(0.30)$ can be coded as 00011001 0000101110 010100101000 00011110 00011110 (The magnitude of the parameters has been ignored). Selection causes the population evolution to approximate toward the desired value. For two randomly candidate solutions, the difference between the response value of the candidate solutions and the desired values of f_r and I_{th} are compared, where the response value is generated by the RSM model. In the comparison, the outstanding individual joins the offspring population. Crossover is at the heart of population evolution and expands the likelihood of model predictions. Similar to biogenetic rules, a new two sets of laser parameter combinations can be generated by swapping a segment of genes between two parent individuals. The purpose of mutation is to increase the diversity of solutions and to prevent the population evolution from falling into a local optimum. Unlike crossover, the process by which variation generates a new combination of laser parameters is to randomly transform 0 and 1 in a gene. It should be noted that the resulting combination of new parameters is constrained by the set boundary, regardless of crossover or mutation. Realistic bounds on each parameter are specified based on known physics of the DFB. Finally, elite retention is the process of preserving better candidate solution from parent to offspring. Fig. 2 represents the specific process of optimization.

III. Result and Discussion

In our simulations, it is considered a DFB laser based on FP laser operating at 1550 nm wavelength, which uses a grating filter to make the device have only one longitudinal mode output [39]. Quantitative and qualitative analysis of key laser parameters is the essential part of the research to optimize laser performance. To avoid the inability of the laser to operate in a single longitudinal mode or the occurrence of spatial hole-burning effects, the grating coupling coefficient is regarded as the ideal value. Due to the coupling of parameters within the DFB laser, simultaneous optimization of multiple parameters of the equivalent circuit model is essential to achieve the desired output characteristics of the laser. Single-factor experiment is an experiment conducted on only one factor, while all other factors are fixed, and it must first be assumed that there are no interactions between the factors. Obtaining the optimal combination of DFB lasers for the desired response with single-factor experiment is a tedious and time-consuming process that cannot be used to study the interaction between laser parameters. Since the small computational effort of the fitted RSM, at least 90% of the time is saved without loss of accuracy. Meanwhile, the results obtained are more stable by combining with the multi-objective optimization of NSGA-II. Thus, determining the optimal combination of laser parameters by combining the RSM model and NSGA-II is a fast and low-cost method.

TABLE I
Sample Point Data

-	Γ	g_0 (10^{-12}m^3/s)	ε (10^{-24}m^3)	R_l	R_r	f_r (GHz)	I_{th} (mA)
1	0.09	4.73	3.26	0.6	0.3	11.482	12.875
2	0.44	4.04	5.45	0.4	0.1	22.909	11.902
…	…	…	…	…	…	…	…
25	0.58	1.76	2.26	0.6	0.3	17.378	12.000
26	0.13	2.44	1.77	0.4	0.5	10.000	13.500
…	…	…	…	…	…	…	…
49	0.19	2.80	15.0	0.6	0.1	12.023	13.642
50	0.18	1.80	12.0	0.3	0.2	9.1201	15.900

A. RSM Model Establishment and Variance Analysis

Sample points are important initial parameters in the RSM calculation, and the reasonable selection of sample points can effectively improve the accuracy of the RSM model. In order to solve the multi-parameter co-optimization of the laser, the constraint bounds of the optimized parameters are determined according to the existing literature as follows: Γ [0.10, 0.70], g_0 [1.0×10^{-12} m^3/s, 8.0×10^{-12} m^3/s], ε [1.0×10^{-24} m^3, 30×10^{-24} m^3], R_l [0.10, 0.70] and R_r [0.10, 0.70], which are extracted from actual DFB lasers [40], [41], [42], [43]. Response value is another important initial parameter in the construction of the response surface model, where the reliability of the model is determined by the accuracy of the response value. Depending on the ranges, 50 sets of sampling points are generated randomly. Simulate the equivalent circuit model by the circuit simulation software PSpice with these sample data, part of the used parameter combinations and the values of the objective responses are given in Table I.

$$\begin{aligned} y_1 = & -15.91583 + 86.19949x_1 + 8.41459x_2 + 0.47517x_3 \\ & + 8.7012x_4 + 26.15468x_5 - 174.70867x_1^2 - 2.06571x_2^2 \\ & - 0.03357x_3^2 + 6.38309x_4^2 - 88.23762x_5^2 + 231.78187x_1^3 \\ & + 0.27566x_2^3 + 0.00139x_3^3 - 26.7918x_4^3 + 156.8775x_5^3 \end{aligned}$$

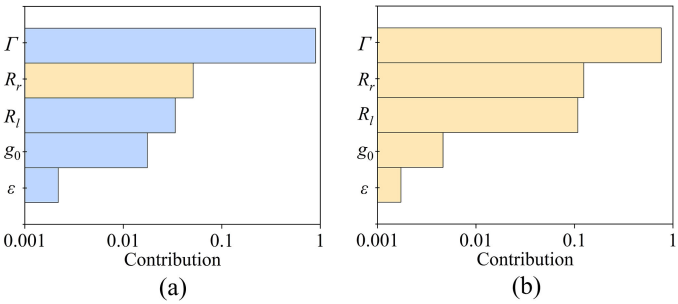

Fig. 3. The contribution of the parameters to (a) Resonant frequency and (b) Threshold current. Blue indicates a positive effect of the parameter on the response, while yellow indicates a negative effect.

$$
\begin{aligned}
&- 129.5993x_1^4 - 0.01369x_2^4 - 0.000002x_3^4 \\
&+ 25.31661x_4^4 - 94.8672x_5^4 + 3.50612x_1 \cdot x_2 \\
&- 1.29016x_1 \cdot x_3 - 16.08955x_1 \cdot x_4 - 7.25145x_1 \cdot x_5 \\
&+ 0.00859x_2 \cdot x_3 - 0.79616x_2 \cdot x_4 - 0.91784x_2 \cdot x_5 \\
&- 0.07895x_3 \cdot x_4 - 0.1051x_3 \cdot x_5 - 5.56419x_4 \cdot x_5
\end{aligned} \tag{10}
$$

$$
\begin{aligned}
y_2 = {} & 35.1883 - 72.20909x_1 - 3.62322x_2 - 0.18591x_3 \\
& -17.7919x_4 - 17.41777x_5 + 196.01537x_1^2 + 0.29574x_2^2 \\
& +0.02321x_3^2 + 1.19467x_4^2 + 15.49495x_5^2 - 306.65109x_1^3 \\
& + 0.00482x_2^3 - 0.00131x_3^3 + 22.58757x_4^3 - 1.57003x_5^3 \\
& + 175.68097x_1^4 - 0.00147x_2^4 + 0.00002x_3^4 \\
& - 19.77102x_4^4 - 8.79996x_5^4 + 1.90094x_1 \cdot x_2 \\
& - 0.00408x_1 \cdot x_3 + 14.47336x_1 \cdot x_4 + 10.45732x_1 \cdot x_5 \\
& - 0.01452x_2 \cdot x_3 + 0.88644x_2 \cdot x_4 + 1.08946x_2 \cdot x_5 \\
& + 0.13695x_3 \cdot x_4 + 0.04393x_3 \cdot x_5 - 0.82459x_4 \cdot x_5
\end{aligned} \tag{11}
$$

The relationship between laser parameters and responses is determined by the ANOVA in terms of regression equations. Two polynomial equations are generated from simulation results using the RSM model for each response. In the above (10)-(11), y_1 and y_2 represent the f_r and I_{th}, respectively. The variables x_1-x_5 correspond to the parameters Γ, g_0, ε, R_l, and R_r. To find the parameters which have the major influence on the laser output characteristics, the normalized model coefficients are transformed into the results of percentage contribution and sensitivity analysis of the parameters based on the RSM model.

Fig. 3 reflects the percent contribution of each parameter to the laser response with positive and negative effects, respectively. The higher the percentage, the higher the contribution of the parameter to the response. Upon comparison, the greatest effect on both resonant frequency and threshold current is Γ, and the least effect is ε. The sensitivity of each parameter is ranked as follows: $\Gamma > R_r > R_l > g_0 > \varepsilon$.

TABLE II
THE CORRELATION COEFFICIENT AND ROOT MEAN SQUARE ERROR RESULT FROM THE OBJECTIVE FUNCTIONS

	f_r	I_{th}
R^2	0.98392	0.93266
σ_{RMSE}	0.03510	0.06761

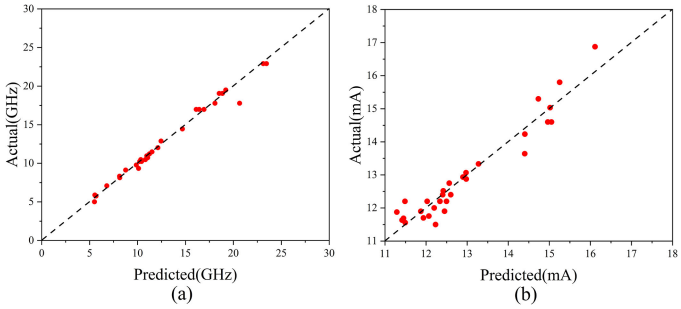

Fig. 4. Results of R^2 analysis for the objective function. (a) Resonant frequency. (b) Threshold current.

The accuracy and credibility of the established model can be measured by ANOVA according to the value of R^2 and σ_{RMSE}. As shown in Table II, the ANOVA of the RSM model showed the high R^2 values for both f_r and I_{th} referring that the RSM model has a high fit. Besides, the σ_{RMSE} of both objective functions is less than 0.1, indicating that the regression of the equations is highly significant. To further demonstrate the model accuracy, the predictive power of the model is tested with 30 additional sample data sets. Fig. 4 shows the comparison results between the predicted and actual values of the objective functions. It can be seen from the figure that the predicted values of both models deviate less from the true values and are closely distributed on both sides of the straight line, which indicates that both established RSM models have high prediction accuracy and can be used for optimization calculations instead of the equivalent circuit model.

The contour plot is used to find a feasible region that, in some sense, optimizes the parameters of laser equivalent circuit model or at least keeps them within desired ranges to search for a combination of parameter levels that simultaneously satisfy the requirements placed on each of the responses and parameters. Each response surface has its own superior region, and the superior region can be further narrowed by superimposing these surfaces. As can be seen from the contour plots in Figs. 5 and 6, for the desired values of f_r and I_{th} to be optimized, superimposed contour plots allow visual determination of the optimization regions where the five parameters are located. Finally, the combination of parameters satisfying both f_r and I_{th} desired values can be determined by the optimization region of the secondary superimposed single target response.

B. Multi-Parameter Optimization Using NSGA-II

Having developed an optimization model and performed a variance analysis, a multi-objective optimization technique is applied to determine the optimum combination of the equivalent

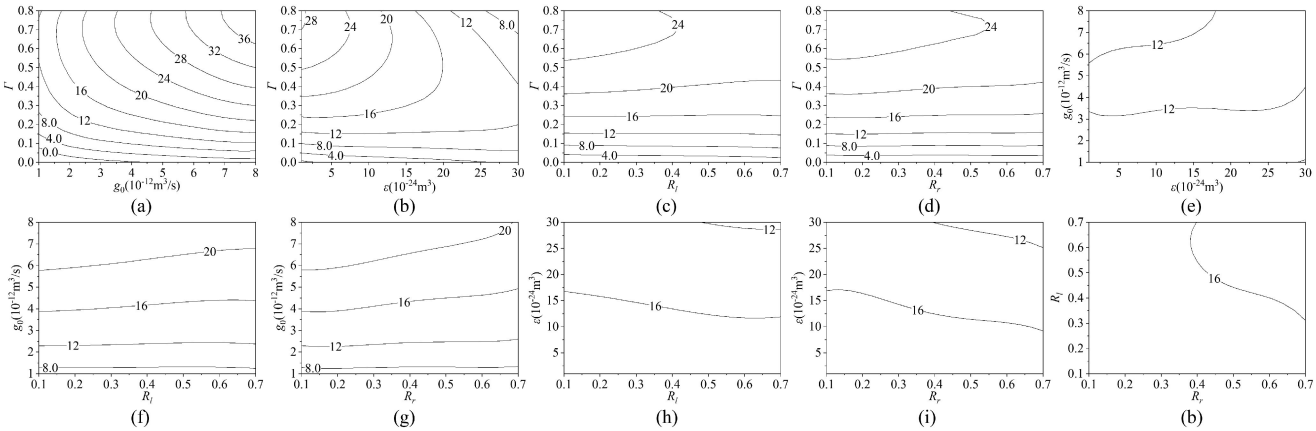

Fig. 5. Contour plot depicting the interaction of (a) Γ and g_0, (b) Γ and ε, (c) Γ and R_l, (d) Γ and R_r, (e) g_0 and ε, (f) g_0 and R_l, (g) g_0 and R_r, (h) ε and R_l, (i) ε and R_r and (j) R_l and R_r for resonant frequency.

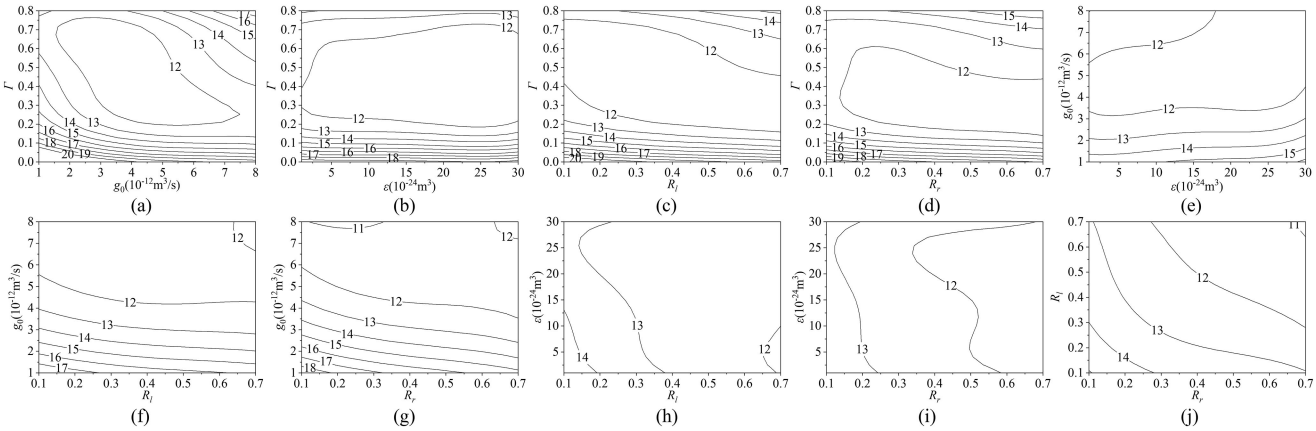

Fig. 6. Contour plot depicting the interaction of (a) Γ and g_0, (b) Γ and ε, (c) Γ and R_l, (d) Γ and R_r, (e) g_0 and ε, (f) g_0 and R_l, (g) g_0 and R_r, (h) ε and R_l, (i) ε and R_r and (j) R_l and R_r for threshold current.

TABLE III
PARAMETERS SETTING OF NSGA-II

Setting	Value
Population Size	20
Number of Generations	12
Crossover Rate	0.9
Variation Period	10
Migration Period	20
Iteration Times	240

circuit model parameters which can produce the best response value. In this paper, the NSGA-II algorithm is used to optimize the established RSM model, which involves a total of five parameter variables and two objective functions. The NSGA-II algorithm is a multi-objective evolutionary algorithm based on the Pareto solution set, and the algorithm converges to the Pareto optimal front end. In NSGA-II, each objective function is treated separately. According to the established optimization model, the parameters of the NSGA-II algorithm are set as shown in Table III.

For the inverse design and parameter optimization of semiconductor lasers, the NSGA-II method allows a fast and efficient search for parameter values corresponding to the desired output characteristics. The characteristics of a laser that has been verified by our research team are selected as the optimization target, with the target values of 12 GHz and 13 mA for the optimized sub-objective functions f_r and I_{th}, respectively [29]. Taking the original parameters of the model as the iterations starting point, the optimization is iterated 240 times. After that, the optimal combination of parameters is continuously searched according to the direction of the operation of the objective function, leading to the feasible solutions set and the optimal solution. It should be noted that the whole optimization process took only 1.5 seconds.

Fig. 7 represents the optimization process diagram of f_r and I_{th}. From the figures, it can be seen that the number of non-dominant solutions occupies the majority in the early stage of the iterative process. Although some mutations are generated during the iterative process, they had little effect on the final optimization results. As the iteration proceeds, the population approaches the Pareto optimal frontier due to the elite retention strategy, which makes the solution approach the target value.

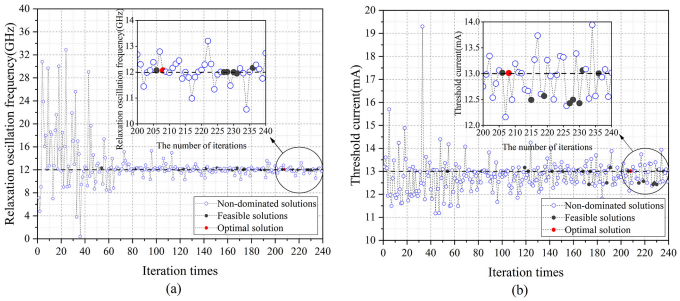

Fig. 7. The iteration process of the objective functions. (a) Resonant frequency. (b) Threshold current.

TABLE IV
COMPARISON OF INITIAL PARAMETERS, OPTIMIZED PARAMETERS AND CALCULATED PARAMETERS

-	Γ	$g_0(\times10^{-12}\mathrm{m}^3/\mathrm{s})$	$\varepsilon(\times10^{-24}\mathrm{m}^3)$	R_l	R_r
S0	0.25	1.42	13.2	0.30	0.30
S1	0.13	4.03	17.9	0.28	0.39
S2	0.14	3.83	16.8	0.39	0.40
S3	0.12	4.16	16.9	0.29	0.39
S4	0.50	1.16	5.78	0.60	0.20
S5	0.70	1.62	8.09	0.40	0.30

Fig. 8 illustrates a 3-dimensional scatter plot, which is a 3-dimensional reduction of a 4-dimensional non-dominated set. Each scatter in the figure represents a set of parameters for a non-dominated solution. In multi-objective optimization of lasers, the design of both response objectives is not optimal at the same time, and the non-dominated set shows the trade-offs between resonant frequency and threshold current. The design feasibility is used to measure the difference between the optimization result and the desired value. The smaller the difference, the higher the design feasibility.

Due to the nonlinear coupling relationship of DFB laser parameters, a set of target responses can correspond to multiple sets of design parameters. Combining RSM with NSGA-II, all parameter combinations on the optimal Pareto front are available as solutions for laser optimization. A comparison of the original parameters and the solutions of the parameters obtained both directly calculated with (5), (6) and applied multi-objective optimization is illustrated in Table IV.

S0 is the initial combination, S1 is the optimal solution, S2 and S3 are feasible solutions, and S4 and S5 are the analytic solutions obtained by direct calculation. The solutions of S1, S2 and S3 are acceptable as they have similar laser parameter values.

The measurement results in Table V are obtained from Table IV. The simulation result of f_r and I_{th} are within 2% error compared to the predicted values, which indicates that the established optimization model has a high degree of fit with the equivalent circuit model. By comparison, the error between the predicted and simulation results for the parameters by direct calculation with (5) and (6) justifies irrational design of the parameters simply applying the formulas for resonant frequency and threshold current, since the integrated effects of the other parameters in the rate equation are entirely ignored. While the error term of the RSM model can compensate well for the effects of other parameters on the output characteristics. The errors are acceptable considering that the RSM model errors lead to inconsistencies between the simulated and desired values of the optimal laser parameters.

TABLE V
COMPARISON OF PREDICTED RESULTS AND SIMULATION RESULTS BETWEEN OPTIMIZATION AND CALCULATION

Solutions	S1	S2	S3	S4	S5
Predicted results of f_r (GHz)	12.064	12.007	12.145	12.000	12.000
Simulation results of f_r (GHz)	12.023	12.023	12.303	11.749	15.488
Predicted results of I_{th} (mA)	13.012	12.995	12.996	13.000	13.000
Simulation results of I_{th} (mA)	13.033	12.752	12.990	16.735	14.898
Error of f_r (GHz)	0.34%	0.13%	1.30%	2.09%	29.1%
Error of I_{th} (mA)	0.16%	1.87%	0.46%	28.7%	14.6%

TABLE VI
COMPARISON OF OPTIMIZATION RESULTS BETWEEN SINGLE-OBJECTIVE OPTIMIZATION AND MULTI-OBJECTIVE OPTIMIZATION

-	Γ	g_0 $(\times10^{-12}\mathrm{m}^3/\mathrm{s})$	ε $(\times10^{-24}\mathrm{m}^3)$	R_l	R_r
Single-objective optimization	0.27	6.93	29.1	0.70	0.24
Multi-objective optimization	0.30	5.98	21.1	0.69	0.34

TABLE VII
COMPARISON OF OPTIMIZATION MODEL PREDICTED RESULTS AND SIMULATION RESULTS BETWEEN SINGLE-OBJECTIVE OPTIMIZATION AND MULTI-OBJECTIVE OPTIMIZATION

	f_r (GHz)	I_{th} (mA)
Predicted results with single-objective	18.033	-
Predicted results with multi-objective	18.004	11.507
Simulation results with single-objective	17.918	11.601
Simulation results with multi-objective	18.107	11.523
Single-objective error	0.64%	-
Multi-objective error	0.57%	0.14%

The multi-objective optimization algorithm can not only reasonably analyze the existing laser parameters and give multiple design solutions, but also optimize the performance of existing devices and make performance predictions. By NSGA-II, the desired response values for f_r and I_{th} are set to 18 GHz and 11.5 mA, respectively. Meanwhile, a comparative analysis between single objective optimization and multi-objective optimization is conducted, and the results are shown in Table VI. To further verify the optimization results, the optimized parameters of both schemes are simulated in the equivalent circuit model, as in Table VII and Fig. 9. Although the current study is based on the same small sample of participants, which results in close threshold current results for single-objective optimization and multi-objective optimization, the results suggest that the subgoal of threshold current is correctly and reasonably chosen. Compared with the single-objective optimization, the multi-objective

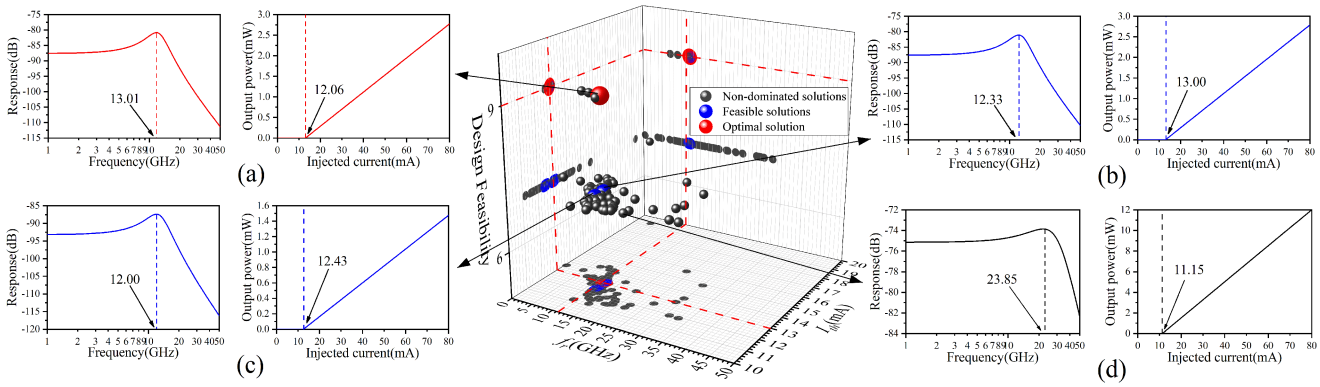

Fig. 8. 3D scatter plot of design feasibility with respect to f_r and I_{th} in the optimization and simulation results with (a) optimal solution, (b) (c) feasible solution and (d) non-dominated solution.

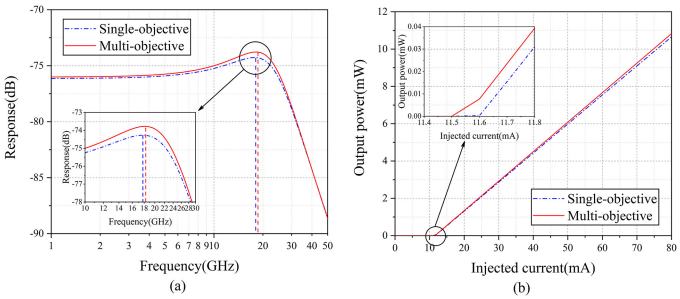

Fig. 9. Simulation of equivalent circuit model with single-objective optimized parameters versus multi-objective optimized parameters. (a) Small-signal frequency characteristic curve (b) Steady-State power versus current characteristics curve.

optimization takes into account the influence of the parameters on the threshold current and achieves further constraints on the parameters, which effectively improves the overall performance of the DFB laser.

The selection of the optimized parameters for this study are several parameters in the single-mode rate equations that have a major impact on the output characteristics of the DFB laser. Whether other more parameters can be optimized by this method remains to be investigated. Furthermore, we would like to include more laser characteristics as additional optimization targets, such as external quantum efficiency, RIN spectra, and noise so that the exact extraction of laser parameters can be achieved by referring to the same method.

IV. Conclusion

In this communication, a parameter optimization method is proposed based on an equivalent circuit model. Multi-objective optimization and the Pareto sorting algorithm are successfully applied to optimize the model's parameters, and model convergence is optimally enhanced. By selecting the regression model, the proposed response surface model with good robustness can fit complex nonlinear responses. The analysis of the resulted optimization model shows that an optimal set of parameters can be rapidly obtained by a finite number of iterations with Pareto preference sorting. Besides, this paper compares and analyses the single-objective optimization method and the multi-objective optimization method. The multi-objective optimization takes the resonant frequency as the optimization objective and further considers the impact of optimization parameters on the threshold current, which is more beneficial to improving the comprehensive performance of the DFB laser.

Therefore, the response surface method is reliable and effective in optimizing the DFB laser parameters. It can not only provide design solutions for optimizing the existing performance of the laser but also guide the reverse design of the laser.

Acknowledgment

The authors would like to thank Professor Wei-ping Huang for his active guidance and valuable suggestions.

References

[1] P. Ma et al., "30-Gbps directly modulated semiconductor lasers based on surface high-order gratings," *IEEE Photon. Technol. Lett.,* vol. 33, no. 4, pp. 197–200, Feb. 2021.

[2] H. M. El-Hageen, P. G. Kuppusamy, A. M. Alatwi, M. Sivaram, and A. Rashed, "Different modulation schemes for direct and external modulators based on various laser sources," *J. Opt. Commun.,* pp. 1–10, 2020, doi: 10.1515/joc-2020-0029.

[3] N. H. Zhu et al., "Directly modulated semiconductor lasers," *IEEE J. Sel. Topics Quantum Electron.,* vol. 24, no. 1, pp. 1–19, Jan./Feb. 2018.

[4] Y. L. Cao, X. N. Hu, Y. B. Cheng, H. Wang, and Q. J. Wang, "Optimization of hybrid silicon lasers for high-speed direct modulation," *IEEE Photon. J.,* vol. 7, no. 2, Apr. 2015, Art no. 1501013.

[5] A. Baylón-Fuentes et al., "Modulation of relaxation oscillation frequency of a DFB laser by using direct detection," in *Proc. SPIE - Int. Soc. Opt. Eng.,* 2011, vol. 7958, pp. 98–105.

[6] K. Uomi, M. Aoki, T. Tsuchiya, M. Suzuki, and N. Chinone, "Dependence of relaxation oscillation frequency and damping K factor on the number of quantum wells in 1.55 mu m InGaAsP DFB lasers," *IEEE Photon. Technol. Lett.,* vol. 3, no. 6, pp. 493–495, Jun. 1991.

[7] J. C. Cartledge and R. C. Srinivasan, "Extraction of DFB laser rate equation parameters for system simulation purposes," *J. Lightw. Technol.*, vol. 15, no. 5, pp. 852–860, May 1997.

[8] A. Melgar, V. A. Thomas, and S. E. Ralph, "Multi-objective laser rate equation based parameter extraction using VCSEL small signal response and RIN spectra," *J. Lightw. Technol.,* vol. 38, no. 23, pp. 6437–6445, Dec. 2020.

[9] S. Loranger, A. Tehranchi, H. Winful, and R. Kashyap, "Realization and optimization of phase-shifted distributed feedback fiber Bragg grating Raman lasers," *Optica,* vol. 5, no. 3, pp. 295–302, 2018.

[10] K. Cheng, L. Xun, and Y. Xi, "Design optimization for 25 Gbps DML InAlGaAs/InP SL-MQW laser diode," in *Proc. Asia Commun. Photon. Conf.*, 2016, Paper AF2A.62.

[11] E. Meland, R. Holmstrom, J. Schlafer, R. B. Lauer, and W. Powazinik, "Extremely high-frequency (24 GHz) InGaAsP diode lasers with excellent modulation efficiency," *Electron. Lett.,* vol. 26, no. 21, pp. 1827–1829, 1990.

[12] J. Y. Wang and M. Cada, "Analysis and optimum design of distributed feedback lasers using coupled-power theory," *IEEE J. Quantum Electron.,* vol. 36, no. 1, pp. 52–58, Jan. 2000.

[13] C. B. Su, V. Lanzisera, R. Olshansky, W. Powazinik, and R. B. Lauer, "15 GHz direct modulation bandwidth of vapour-phase regrown 1.3 μm InGaAsP buried-heterostructure lasers under CW operation at room temperature," *Electron. Lett.,* vol. 21, no. 13, pp. 577–579, 1985.

[14] C. B. Su, V. Lanzisera, W. Powazinik, E. Meland, R. Olshansky, and R. B. Lauer, "12.5-GHz direct modulation bandwidth of vapor phase regrown 1.3-μm InGaAsP buried heterostructure lasers," *Appl. Phys. Lett.,* vol. 46, no. 4, pp. 344–346, 1985.

[15] R. Olshansky, V. Lanzisera, C. B. Su, W. Powazinik, and R. B. Lauer, "Frequency response of an InGaAsP vapor phase regrown buried heterostructure laser with 18 GHz bandwidth," *Appl. Phys. Lett.,* vol. 49, no. 3, pp. 128–130, 1986.

[16] R. Olshansky, W. Powazinik, P. Hill, V. Lanzisera, and R. B. Lauer, "InGaAsP buried heterostructure laser with 22 GHz bandwidth and high modulation efficiency," *Electron. Lett.,* vol. 23, no. 16, pp. 839–841, 1987.

[17] W. W. Chow, Y. Wan, J. E. Bowers, and F. Grillot, "Analysis of the spontaneous emission limited linewidth of an integrated III–V/SiN laser," *Laser Photon. Rev.*, vol. 16, 2022, Art. no. 2100620.

[18] C. Zhang, S. Yan, Q. J. Zhang, and J. G. Ma, "Behavioral modeling of power amplifier with long term memory effects using recurrent neural networks," in *Proc. IEEE Int. Wireless Symp.*, 2013, pp. 1–4.

[19] X. Sun et al., "Design and optimization of 1.55 μm algainas MQW polarization mode controllers," *Photonics,* vol. 8, no. 10, pp. 1–11, 2021.

[20] W. Quan, X. Li, J. Liu, K. Shen, and Y. Zhai, "Genetic algorithm for accurate modeling of distributed Bragg reflector laser power and wavelength," *Opt. Eng.,* vol. 58, no. 2, 2019, Art. no. 026108.

[21] R. Woodward and E. J. Kelleher, "Towards 'smart lasers': Self-optimisation of an ultrafast pulse source using a genetic algorithm," *Sci. Rep.,* vol. 6, no. 1, pp. 1–9, 2016.

[22] P. Szczepanski, "Approximate analysis of nonlinear operation of a distributed feedback laser," *Appl. Opt.,* vol. 24, no. 21, pp. 3574–3578, 1985.

[23] T. Simpson, "Mapping the nonlinear dynamics of a distributed feedback semiconductor laser subject to external optical injection," *Opt. Commun.,* vol. 215, no. 1–3, pp. 135–151, 2003.

[24] P. Szczepański, "Approximate analysis of nonlinear operation of a distributed feedback laser with parasitic losses," *J. Appl. Phys.,* vol. 63, no. 10, pp. 4854–4859, 1988.

[25] H.-F. Liu and W. F. Ngai, "Nonlinear dynamics of a directly modulated 1.55 mu m InGaAsP distributed feedback semiconductor laser," *IEEE J. Quantum Electron.,* vol. 29, no. 6, pp. 1668–1675, Jun. 1993.

[26] B. Acherjee, A. S. Kuar, S. Mitra, and D. Misra, "Modeling and analysis of simultaneous laser transmission welding of polycarbonates using an FEM and RSM combined approach," *Opt. Laser Technol.,* vol. 44, no. 4, pp. 995–1006, 2012.

[27] R. GUO et al., "Using response surface methodology (RSM) to optimize the key laser processing parameters for laser cladding of grey cast iron," *Lasers Eng.,* vol. 51, pp. 75–95, 2021.

[28] M. Shahine and Y. J. Chen, "Analysis for commanding the self-pulsation of DFB laser diode with electronic feedback for photonic analog-to-digital conversion application," *IEEE Photon. J.,* vol. 2, no. 6, pp. 1013–1026, Dec. 2010.

[29] B. Nie et al., "Circuit model for the effect of nonradiative recombination in a high-speed distributed-feedback laser," *Curr. Opt. Photon.,* vol. 4, no. 5, pp. 434–440, 2020.

[30] F. Habibullah and W.-P. Huang, "A self-consistent analysis of semiconductor laser rate equations for system simulation purpose," *Opt. Commun.,* vol. 258, no. 2, pp. 230–242, 2006.

[31] R. H. Myers, D. C. Montgomery, and C. M. Anderson-Cook, *Response Surface Methodology: Process and Product Optimization Using Designed Experiments*. Hoboken, NJ, USA: Wiley, 2016.

[32] B. Keshtegar, S. Heddam, O. Kisi, and S.-P. Zhu, "Modeling total dissolved gas (TDG) concentration at Columbia river basin dams: High-order response surface method (H-RSM) vs. M5Tree, LSSVM, and MARS," *Arabian J. Geosci.,* vol. 12, no. 17, pp. 1–15, 2019.

[33] C. Li, J. Huang, K. Wang, Z. Chen, and Q. Liu, "Optimization of processing parameters of laser skin welding in vitro combining the response surface methodology with NSGA-II," *Infrared Phys. Technol.,* vol. 103, 2019, Art. no. 103067.

[34] C. Senthilkumar, G. Ganesan, and R. Karthikeyan, "Optimisation of ECM parameters using RSM and non-dominated sorting genetic algorithm (NSGA II)," *Int. J. Machining Machinability Mater.,* vol. 14, no. 1, pp. 77–90, 2013.

[35] W. Deng et al., "An enhanced fast non-dominated solution sorting genetic algorithm for multi-objective problems," *Inf. Sci.,* vol. 585, pp. 441–453, 2022.

[36] S. Mirjalili, "Genetic algorithm," in *Evolutionary Algorithms and Neural Networks*. Springer, 2019, pp. 43–55.

[37] M. Kumar, D. Husain, N. Upreti, and D. Gupta, "Genetic algorithm: Review and application," *Available at SSRN 3529843,* 2010.

[38] K. Deb, A. Pratap, S. Agarwal, and T. Meyarivan, "A fast and elitist multiobjective genetic algorithm: NSGA-II," *IEEE Trans. Evol. Computation*, vol. 6, no. 2, pp. 182–197, Apr. 2002.

[39] Q. Ding et al., "Continuous current-injected waveforms shaping for suppressing relaxation oscillations of direct modulation based on equivalent circuit model," *Opt. Exp.,* vol. 30, no. 11, pp. 19273–19287, 2022.

[40] W. Feng and N. J. O. Zhu, "Analysis of chirp characteristics of DFB lasers and integrated laser-modulators," *Opt. Quantum Electron.,* vol. 36, no. 14, pp. 1237–1245, 2004.

[41] S. S. Ghoniemy, S. Mahmoud, and L. MacEachern, "Semi-analytical semiconductor parameters extraction algorithm for optical link simulations," in *Proc. Nat. Radio Sci. Conf.*, 2009, pp. 1–5.

[42] J. Gao, "High frequency modeling and parameter extraction for vertical-cavity surface emitting lasers," *J. Lightw. Technol.*, vol. 30, no. 11, pp. 1757–1763, Jun. 2012.

[43] P. André et al., "Extraction of laser parameters for simulation purposes," in *Proc. 5th Int. Conf. Numer. Simul. Optoelectron. Devices*, 2005, pp. 103–104.